

Layered double hydroxide modified polyamide reverse osmosis membrane for improved permeability

Wei-Liang Liu, Jia-Ming Gao, Zhi-Hao Huang, Hao Zhang, Meng-Ping Li, Xin Zhang, Xiao-Hua Ma*, Zhen-Liang Xu

Shanghai Key Laboratory of Multiphase Materials Chemical Engineering, Membrane Science and Engineering R&D Lab, Chemical Engineering Research Center, School of Chemical Engineering, East China University of Science and Technology, 130 Meilong Road, 200237, Shanghai, China, Tel. +86 21 64253670; Fax: +86 21 64252989; email: xiaohuama@ecust.edu.cn (X.-H. Ma)

Received 5 January 2020; Accepted 5 June 2020

ABSTRACT

Layered double hydroxides (LDHs) are typical two-dimensional nanomaterials, which can be easily modified to serve molecular transport channels for improving membrane's performances. In this study, two types of LDHs, namely citric acid (CA) intercalated LDHs and carbon dots (CDs) intercalated LDHs, have been synthesized and used as nonfillers to modify polyamide (PA) thin-film composite reverse osmosis membranes. The influence of different concentrations of LDHs on the physicochemical properties and morphologies of the RO membranes was investigated. The chemical composition of the membranes was measured by Fourier transform infrared spectroscopy and the morphologies of the modified RO membranes were studied by scanning electron microscopy, transmission electron microscopy, and atomic force microscopy. The obtained membranes exhibited sparser leaf-like structures, resulting in a flux of $33.2 \text{ L m}^{-2} \text{ h}^{-1}$, approximately 36% improvement compared with the unmodified membrane. Our results showed that LDHs modified PA membranes could effectively improve the permeability of the membrane.

Keywords: Layered double hydroxides; Polyamide TFC membrane; Carbon dots; Morphology; Permeability

1. Introduction

Nowadays, reverse osmosis (RO) technology is one of the most widely used technologies for solving the water supply shortage [1,2]. RO is a water treatment process driven by pressure whereby a semi-permeable membrane rejects dissolved constituents in the feeding water but allows water to pass through [3]. A typical RO membrane is usually fabricated by a reaction on a porous substrate called interfacial polymerization (IP) between an acyl chloride monomer and an amine monomer, which usually are trimesoyl chloride (TMC) and *m*-phenylenediamine (MPD), respectively [4–6]. The performance of a RO membrane is strongly determined by the properties of the polyamide (PA) thin films formed

by the IP reaction. Incorporating porous materials with nanochannels in the PA thin film of RO membrane has been proved to be a promising way to fabricate high-performance membrane [7–9].

Layered double hydroxide (LDHs), which have a lamellar structure with exchangeable interlayer anions, is one type anionic layered organic materials generally composed of two metal oxy-oxides. The chemical composition of the main layer, as well as the type and quantity of the interlayer anions are controllable, endowing LDHs with many unique physicochemical properties such as high aspect ratio and controllable assembly [10,11]. Compared with other nanochannel materials like carbon nanotubes (CNTs), graphene oxide (GO), and aquaporin, LDHs have a large advantage

* Corresponding author.

in relatively convenient fabrication and much lower cost, which can reduce the cost in membrane production.

In previous studies, LDHs have been used as nanofillers in membrane to improve separation performance by shortening the mass transfer distance [12] and enhancing mechanical strength of the membrane [13–15], emulsifying agents to facilitate the diffusion rate of MPD from the aqueous phase to the organic phase [16–18], and they are also used as water carriers to enhance the hydrophilicity of the membrane because of the hydration of ions [19]. Nevertheless, LDHs are apt to aggregate especially when they are dried, resulting in difficulty in dispersing in water, which really limits their application. Methoxide LDHs, LDHs prepared in methanol, can disperse well in water through complete hydrolysis of the alkoxide ion [20,21]. Therefore, methoxide LDHs were synthesized in this work to produce a uniformly distributed nanochannel in membrane.

Carbon dots (CDs) with a GO-like structure but with much smaller particle size [22] are more stable when dispersing in water. Citric acid (CA), as a cheap organic acid with plentiful carboxyl groups, has become an ideal precursor to produce CDs. CA can be intercalated into LDHs through anion exchange between citrate and another weaker-binding anion, that is, NO_3^- . Through a hydrothermal reaction, citrate intercalated in LDHs can form CDs by *in-situ* self-assembling into sheet structure followed by condensation reactions through intermolecular reaction, CA molecules can dihydroxylation [23]. CDs obtained from CA possess excellent hydrophilicity due to their plenty of oxygen-containing functional groups like hydroxyl and carboxyl groups [24]. The influence of CA and CD on LDHs, as well as on the PA TFC membranes was very interesting and required to further investigate.

Herein, two types of methoxide LDHs with a better dispersion ability in water, namely CA intercalated LDHs and CDs intercalated LDHs, were prepared through a fast nucleation and slow aging method and used as nonfillers to modify the PA membrane. The structure and chemical composition of LDHs were characterized. Then the prepared LDHs were added into aqueous phase to fabricate TFC RO membrane through IP reaction. The membrane properties (i.e., separation, morphology, and hydrophilicity) were measured and the influence of LDHs amount was investigated.

2. Experimental

2.1. Materials

$\text{Mg}(\text{NO}_3)_2 \cdot 6\text{H}_2\text{O}$ (AR), $\text{Al}(\text{NO}_3)_3 \cdot 9\text{H}_2\text{O}$ (AR), NaOH (AR), citric acid (≥ 98 wt.%), ethylenediamine (EDA, AR), and MPD (≥ 98 wt.%) were purchased from Shanghai Macklin Biochemical Co., Ltd., (Shanghai, China). NaCl (AR), Methanol (AR), and hexane (AR) were purchased from Shanghai Titan Scientific Co., Ltd., (Shanghai, China). TMC (≥ 98 wt.%) was supplied by Qingdao Benzo Chemical Company (Qingdao, China). The supporting membranes, polysulfone (PSF) UF membrane (the molecular weight cut off and pure water flux are $50,000$ Da and $300 \text{ L m}^{-2} \text{ h}^{-1} \text{ bar}^{-1}$, respectively), were obtained from the development center for water treatment technology (Hangzhou, China). Deionized water was used in all the experimental processes.

2.2. Membrane fabrication

2.2.1. Preparation of CA intercalated LDHs

Citric acid anion intercalated Mg–Al LDHs, with an Mg/Al molar ratio of 2, were synthesized via a fast nucleation and slow aging method [25]. Typically, $0.02 \text{ mol Mg}(\text{NO}_3)_2 \cdot 6\text{H}_2\text{O}$ and $0.01 \text{ mol Al}(\text{NO}_3)_3 \cdot 9\text{H}_2\text{O}$ were dissolved in a three-neck with 100 mL methanol. Then the solution was heated to 65°C in water bath with a stirring speed of 300 rpm . After that, 0.07 mol NaOH and 0.01 mol CA were added in 100 mL methanol and ultrasonically treated for 30 min for complete dissolving. The above solution was added into the three-neck flask and aged at 65°C with stirring for 72 h . The resulting precipitate was separated by centrifugation and thoroughly rinsed to reach a neutral pH value, followed by drying in an oven at 60°C for 6 h . The final product was denoted as CA-LDHs.

2.2.2. Preparation of CD intercalated LDHs

Carbon dot intercalated LDHs were prepared via an *in-situ* hydrothermal reaction between EDA and CA intercalated in the CA-LDHs [26]. Briefly, 0.4 g CA-LDHs and 0.02 mL EDA were dissolved 40 mL methanol. The suspension was put into a teflon-lined autoclave and hydrothermally treated at 150°C for 6 h . The resulting product was centrifuged, washed with methanol, and air-dried in an oven at 60°C for 6 h . The final product was denoted as CD-LDHs.

2.2.3. Preparation of TFC membranes

The TFC membranes were fabricated by the IP reaction. Aqueous solution was prepared by dispersing certain amounts of CA-LDHs and CD-LDHs in $2 \text{ wt.}\%$ MPD solution, respectively. Organic solution was prepared by adding TMC in *n*-hexane with a concentration of $0.2 \text{ wt.}\%$. After ultrasonically treated for 30 min , aqueous solution was poured on the top surface of PSF substrate. After being soaked for 5 min , the excess aqueous solution was carefully removed from the PSF top surface. Subsequently, a soft rubber roller was used to remove residual droplets on the surface. Afterward, the top surface was exposed to the organic solution for 1 min to form a thin polyamide film on PSF substrate by reaction between TMC and MPD. After the reaction, the thin polyamide layer was immediately washed with sufficient hexane. After a heat treatment by placing the membrane in 50°C deionized water for 10 min , the resulting RO membrane was stored in deionized water before further tests. The thin film nanocomposite (TFN) RO membranes prepared by aqueous solution with CA-LDHs contents of 0.005 , 0.020 , $0.050 \text{ wt.}\%$ were designated as CA-05, CA-20, and CA-50, respectively. The TFN RO membranes prepared by aqueous solution with CD-LDHs contents of 0.005 , 0.020 , $0.050 \text{ wt.}\%$ were designated as CD-05, CD-20, and CD-50, respectively. The RO membrane prepared by aqueous solution without LDHs was designated as M0.

2.3. Characterization

Chemical compositions of LDHs were characterized by Fourier transform infrared spectroscopy (FT-IR, Nicolet

5700, Thermo Electron Corp., Pittsburgh, PA, USA). The crystal structures of LDHs were investigated by X-ray diffraction (XRD, D8 Advance, Bruker Corporation, Billerica, MA, USA). The morphologies of LDHs were visualized by scanning electron microscope (SEM, NOVA NANOSEM450, FEI Corporation, Hillsboro, OR, USA). Membrane morphologies were observed by SEM. FT-IR spectroscopy was used to study the chemical compositions of RO membranes. XRD were used to investigate the inner structure of RO membranes. Atomic force microscopy (AFM, Nanoscope IIIa Multimode AFM, Veeco, Plainview, NY, USA) with $5 \mu\text{m} \times 5 \mu\text{m}$ scanning range was used to determine the roughness of top surface and R_a (arithmetic mean roughness) were analyzed by software Nanoscope. Dynamic water contact angle was evaluated by contact angle meter (JC2000A, Shanghai Zhong Cheng Digital Equipment Co., Ltd., China) at 25°C .

2.4. RO performance test

The flux and rejection performance of RO membranes were tested by a cross-flow filtration system. The effective area of membrane is 22.5 cm^2 . And the system was operated under pressure of 1.6 MPa with a cross-flow velocity of 22.4 cm/s. The RO membranes were initially compacted for 1 h to reach a steady state. A 2,000 mg/L NaCl solution was used in rejection performance test. The temperature of solution in this system was maintained at $24^\circ\text{C} \pm 0.1^\circ\text{C}$ through a circulating chiller. The permeation flux of pure water was calculated as follows:

$$J_w = \frac{V}{A_m \times \Delta t} \quad (1)$$

where J_w is the permeation flux ($\text{L m}^{-2} \text{ h}^{-1}$), V is the volume of permeated water (L), A_m is the effective membrane area (m^2), and Δt is the collection time (h) of permeated water.

The salt rejection was calculated by the following equation:

$$R = \left(1 - \frac{C_p}{C_f} \right) \times 100\% \quad (2)$$

where C_p and C_f are the permeate concentration and the feed concentration of salt solution, respectively. The concentrations of NaCl were measured by DDS-307A conductance meter (Shanghai Neici Instrument Company, China).

3. Results and discussion

3.1. Characterization of LDHs

The FT-IR spectrum of CA-LDHs and CD-LDHs are shown in Fig. 1. The strong wide peaks at 3425 cm^{-1} represented the stretching vibration of O–H, proving the existence of bound water between layers. Carboxyl group of citric acid was confirmed by the intense peaks at 1,635 and $1,380 \text{ cm}^{-1}$ which were attributed to vibration absorption from the C=O band of asymmetric and symmetric carboxylate anion, demonstrating that nitrate between layers was successfully replaced by citric acid. The peaks at 1,298 and $1,255 \text{ cm}^{-1}$ belonged to C–O. And the vibration band of the methylene

group at $2,848 \text{ cm}^{-1}$ indicated the successful intercalation and reaction of EDA with CA-LDHs.

The prepared methoxide CA-LDHs and CD-LDHs can form a stable and homogeneous suspension in water (Fig. 2a). This is mainly because the methoxide LDHs can combine with water to form colloids to disperse well in water. When irradiated with ultraviolet light at 365 nm, CD-LDHs could emit a blue light (Fig. 2b), which was ascribed to the specific fluorescence of carbon dots intercalated in CD-LDHs, proving citrate successfully transform to carbon dots under high temperature. After 6 h of standing, CA-LDHs had settled to the bottom of bottle while CD-LDHs remained a homogeneous suspension (Fig. 2c). That means, though intercalated in layers, anions still had a strong influence on property of LDHs. The superior dispersion of CD-LDHs in water was due to the super-hydrophilic carbon dots intercalated in layers, which largely enhanced its water affinity.

The SEM images in Fig. 3 shows the morphology of CA-LDHs and CD-LDHs. CA-LDHs and CD-LDHs both have a thin nanosheet structure, which is the typical feature for LDHs made by magnesium and aluminium [10]. However, CD-LDHs had a severer agglomeration after drying, forming rose-like aggregates. The length of CA-LDHs ranged from 45 to 150 nm, and most of the LDHs were $<90 \text{ nm}$, which were much smaller than LDHs reported in previous works [11]. Compared with CA-LDHs, CD-LDHs had a larger length about 96 nm in average. The thickness of the LDHs was less than 25 nm. The smaller particle size may result from the methoxyl producing in reacting in methanol, which prevented the LDHs from aggregation during aging process.

The XRD patterns of CA-LDHs and CD-LDHs are shown in Fig. 4a. The diffraction peaks at 2θ values of 11.6° (003), 23.1° (006), 34.5° (009), 38.5° (015), 46.1° (018), 60.7° (010), and 61.9° (013) were found on CA-LDHs and CD-LDHs, which were consistent with the standard XRD peaks for Mg/Al-LDHs, indicating that the well crystallized LDHs had been synthesized in this work [19,27]. The d003-spacing of the CD-LDHs and CA-LDHs was calculated as 0.75 and 0.76 nm, respectively, according to the Bragg's

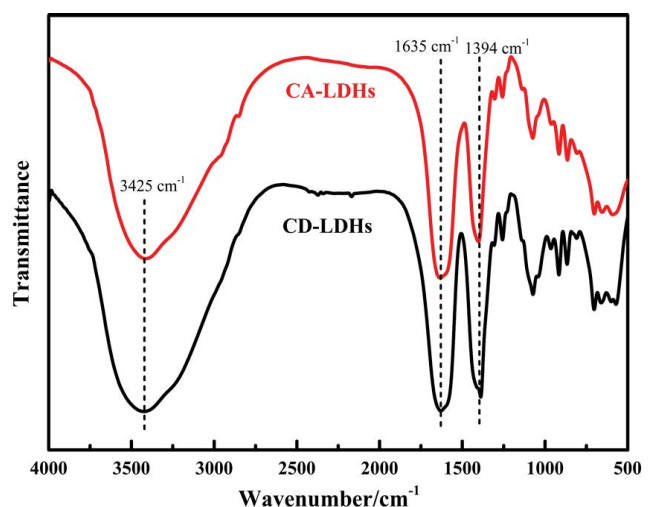


Fig. 1. FT-IR spectra of CA-LDHs and CD-LDHs.

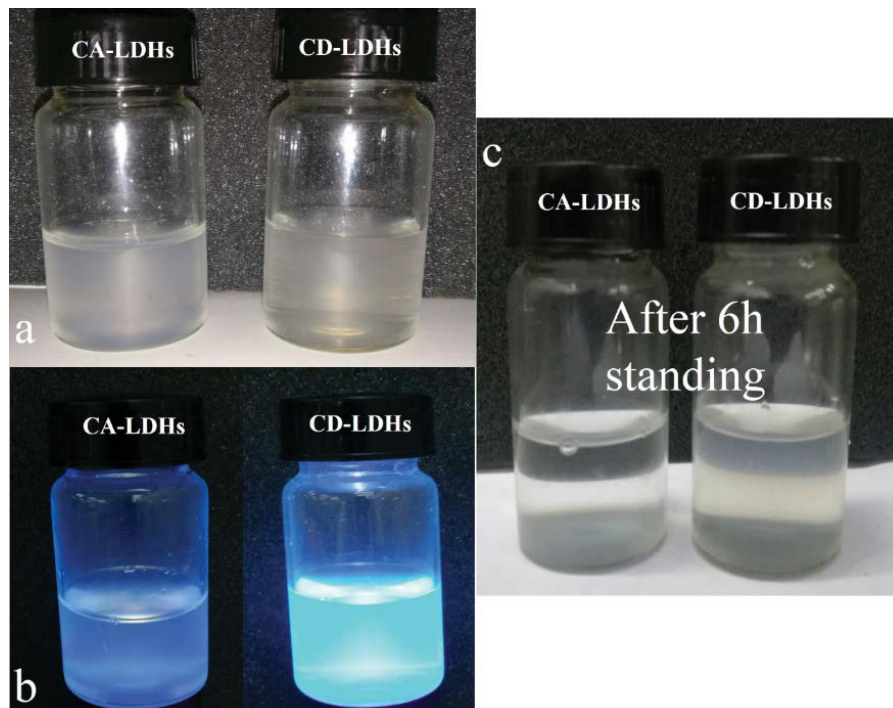


Fig. 2. Photos of suspension solutions of (a) 0.5% (w/w) CA-LDHs and CD-LDHs in water, (b) irradiated with ultraviolet light at 365 nm, and (c) after 6 h standing.

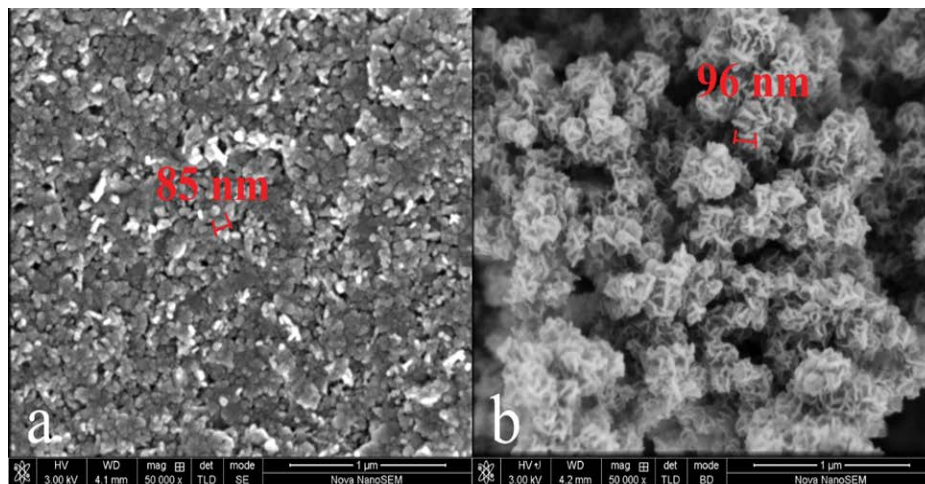


Fig. 3. SEM images of (a) CA-LDHs and (b) CD-LDHs.

law. This dicates that citric acid dehydration and condensation into carbon dots reduce the interlayer spacing of LDHs. The diffraction peak of CD-LDHs was stronger than CA-LDHs, revealing that the crystallinity of CD-LDHs was improved because of a further high temperature process.

3.2. Characterization of RO membranes

The XRD patterns of LDHs modified membranes are shown in Figs. 4b and c. All membranes presented three diffraction peaks which could be observed in polyamide. The hydroxyl groups of the intercalated anion exist in

LDHs can react with acyl chloride bond of TMC, leading to a chemical combination between LDHs and polyamide. The combination in crystal lattice eventually resulted in a deformation of the lattice, which could be verified by the broad peak at 13.7°. The peak could be attributed to the migration of diffraction peak of LDHs at 11.7°. As the amount of LDH added increasing, the peak became wider, indicating that CA-LDHs and CD-LDHs were combined with membranes successfully.

Fig. 5 shows the morphology of top surface of RO membrane prepared with different CA-LDHs contents in aqueous phase. In Fig. 5, all membranes present a typical

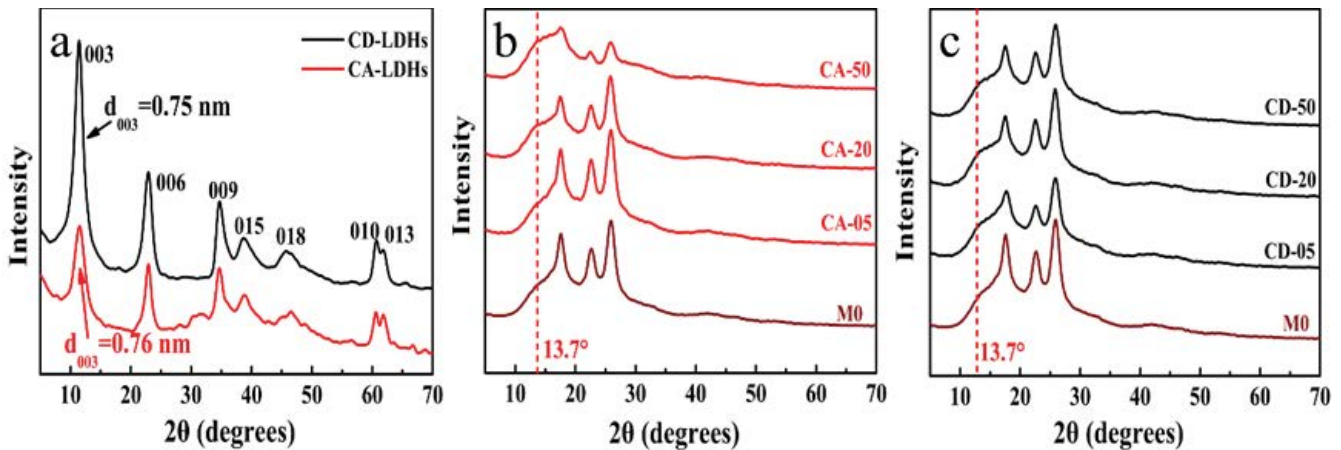


Fig. 4. XRD patterns of (a) CA-LDHs and CD-LDHs, (b) CA-LDHs modified membranes, and (c) CD-LDHs modified membranes.

leaf-like structure or ridge-and-valley structure [28] usually existed in PA RO membrane prepared by TMC and MPD. And these leaf-like structures varied with different CA-LDHs contents. When CA-LDHs was not added (M0), the structure mainly consisted of large amount of close-packed long strips and little nodules between strips (Fig. 5a2). For the membrane prepared by aqueous phase containing 0.005% CA-LDHs (CA-05), the strips arranged more sparsely. Compared with M0, there were more nodule-like structures in CA-05. A larger and sparser leaf-like structure with curly edges could be found in Fig. 5c, as the CA-LDHs content increased to 0.02% (CA-20). In Fig. 5d2, much more nodules appeared with more CA-LDHs content. By comparing the SEM images in Fig. 5, we could find that the leaf-like structures were getting smaller when the amount of CA-LDHs ascended.

The morphology of RO membrane prepared with CD-LDHs in aqueous phase was also investigated in Fig. 6. Compared with CA-20, a tighter and thicker leaf-like structure was observed on the top surface of CD-20. According to the TEM result in Fig. 6, the PA layer of CA-20 had the largest average thickness with little fluctuation. Many cavities or empty spaces were observed in the PA layer, which was corresponding to the top surface structure well. Meanwhile, the CD-20 showed a much denser PA layer both in SEM and TEM image, which proved that CD-LDHs had a different infection on IP process.

AFM images of CA-LDHs modified membrane with $5 \mu\text{m} \times 5 \mu\text{m}$ scanning range are presented in Fig. 5. CA-05 had the roughest top surface while CA-20 had the smoothest surface. The roughness parameters followed the order: CA-05 > M0 > CA-50 > CA-20. The variation in roughness was corresponding to the morphology diversity observed in SEM images in Fig. 5.

Combined with SEM result, we can find that compared with nodule-like structure, a sparse leaf-like structure can result in a smaller contact angle (Fig. 7a), which usually means a better hydrophilia. Particularly, though carbon dots had an excellent hydrophilicity, CD-05 and CD-20 didn't show an enormous decline in contact angle like other highly hydrophilic materials modified membrane. On the contrary, the contact angle showed a little rise. It could be speculated

that LDHs are all under PA layer at low addition, so the contact angle is still determined by surface morphology. With the addition increasing, CD-50 showed an apparent decline in contact angle, indicating that carbon dots were exposed to the surface of membrane.

Figs. 8a and c show the attenuated total reflection-Fourier transform infrared (ATR-FTIR) spectra of RO membrane with different LDHs contents. The typical bands of polyamide prepared by TMC and MPD were observed clearly in spectra. The bands at about $1,660$ and $1,547 \text{ cm}^{-1}$ were characteristic of a C=O stretch and a C-N stretch, respectively, indicating the existence of amide bond. The band at $1,610 \text{ cm}^{-1}$ was ascribed to the absorption peak of polyamide aromatic ring. The bands at $1,587$ and $1,245 \text{ cm}^{-1}$ were characteristic bands for PSF. The amount of PA layer could be evaluated by the area ratio of peak at $1,660 \text{ cm}^{-1}$ to peak at $1,245 \text{ cm}^{-1}$ [29,30]. The ratio (the peak area ratio of $1,660$ and $1,245 \text{ cm}^{-1}$ wavenumber) in Fig. 8b showed a tendency to rise first and then fall. We can presume that the PA layer thickness of the CA-LDHs modified membranes first increases as the amount of CA-LDHs increases and then declines when the amount of CA-LDHs continues to increase. Associated with the SEM and TEM images in Fig. 6, it could be proved that the larger leaf-like structure contributed to the increase in thickness, since CA-20 with a thicker loose PA layer had a larger ratio than M0 while CD-20 with a dense but thinner PA layer had a smaller ratio.

The variation in morphology is attributed to the variation of the diffusion rate of MPD from the aqueous phase to the organic phase. During an interfacial polymerization reaction, a loose polymer film will generate first in the reaction zone [31]. The reaction zone normally exists in organic phase because of a better diffusion for MPD. A larger MPD diffusion means the reaction zone is farther from the interface between two phases and this cause a larger and sparser leaf-like structure (Fig. 9). When dispersing in water, LDHs can combine with water and form colloid. The colloid LDHs provide a transport channel between aqueous phase and reaction zone, making MPD molecule easier to reach the reaction. More available MPD molecules in the reaction zone increase the amine to acyl chloride molar ratio and promote the polymerization rate [32–34], resulting in

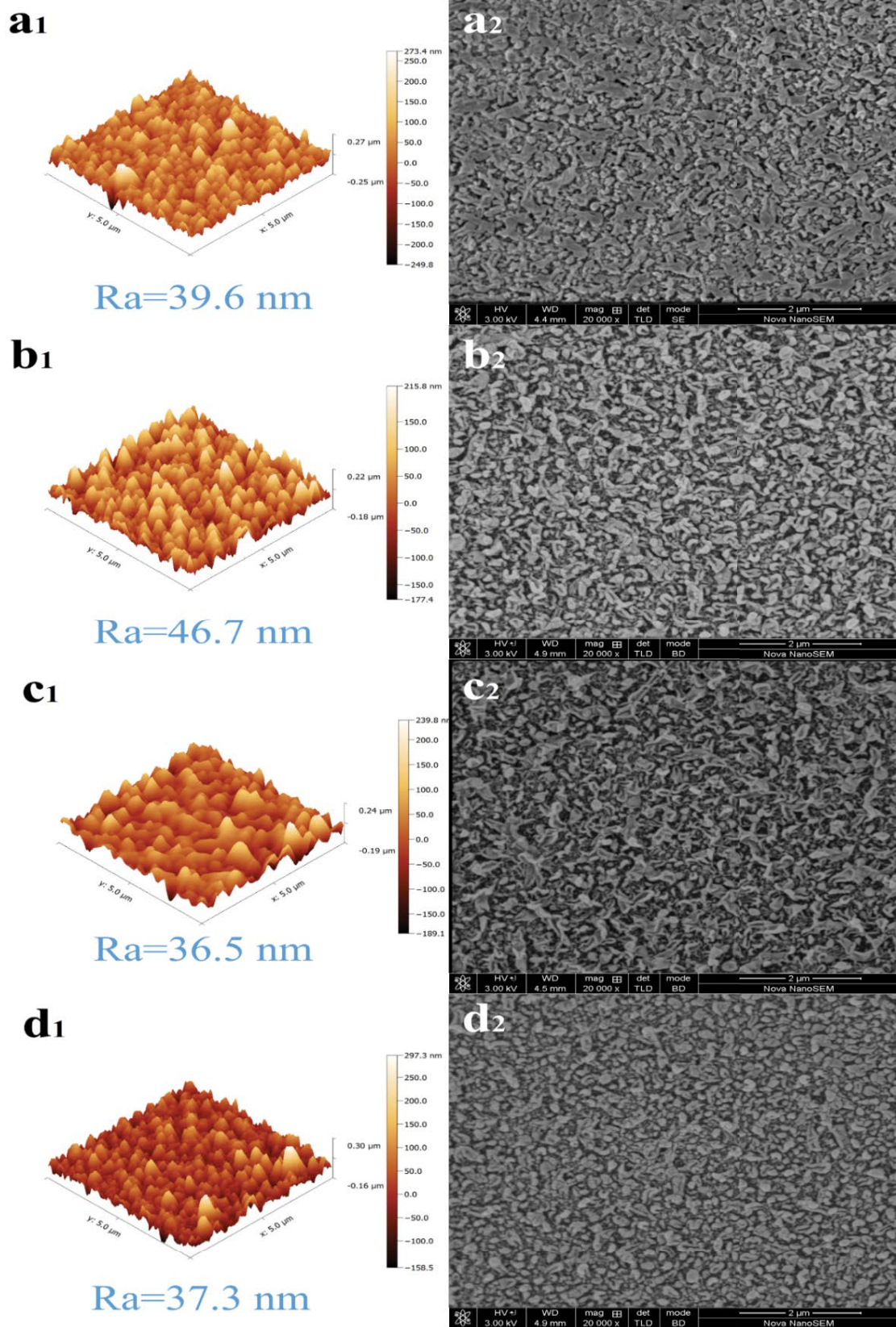


Fig. 5. SEM and AFM images of the top surface of PA TFC membrane with different CA-LDHs concentrations (a) M0, (b) CA-05, (c) CA-20, and (d) CA-50.

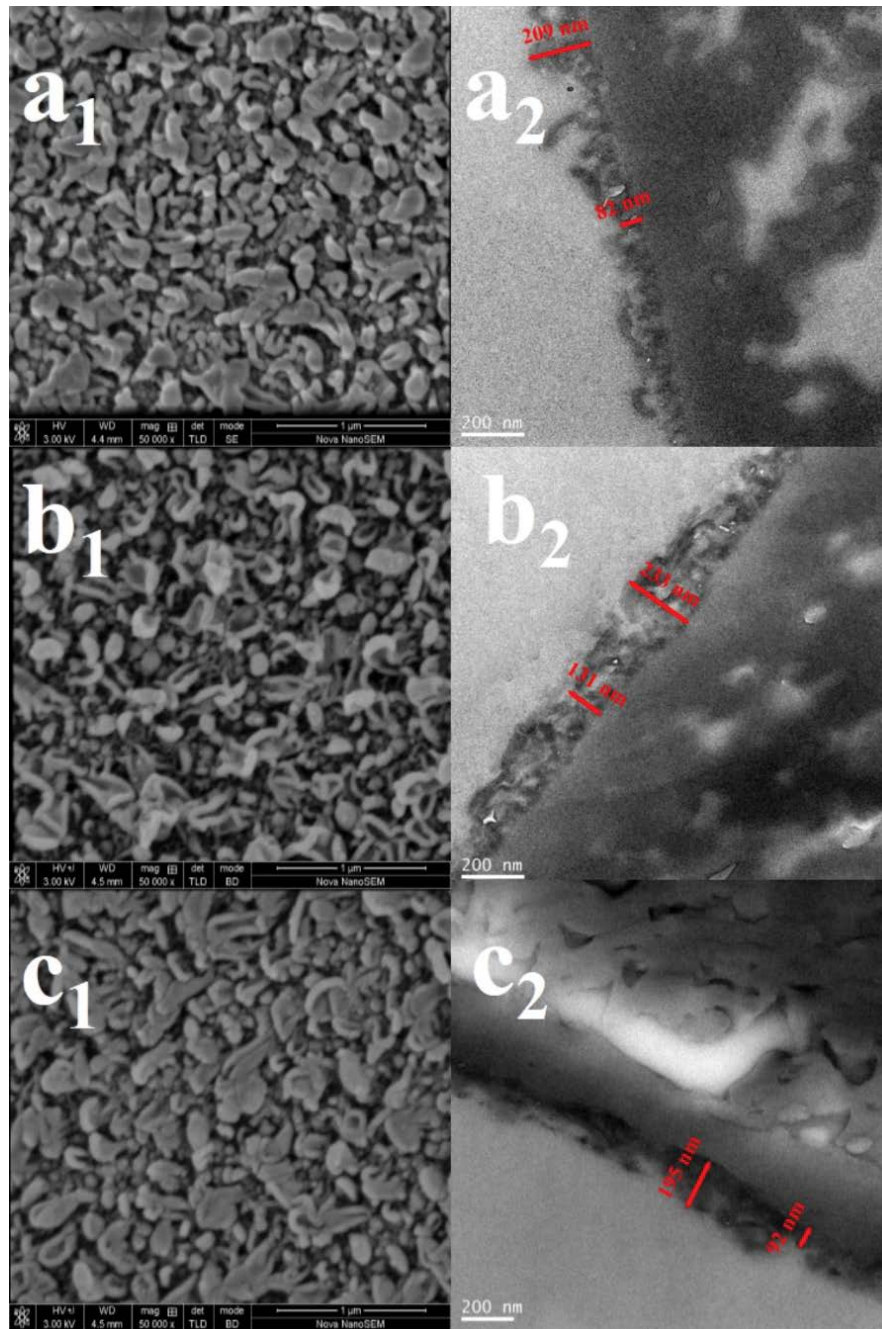


Fig. 6. SEM image of the top surface and TEM image of section of PA TFC membrane: (a) M0, (b) CA-20, and (c) CD-20.

widespread structures and thicker PA layers, that is, leaf-like structures found in CA-05 and CA-20. According to the ATR-FTIR and TEM results, all CD-LDHs modified membranes had a thinner PA layer. The diverse morphologies could be explained by the process described in Fig. 9. CD-LDHs have a larger improvement on MPD diffusing rate because of a better hydrophilicity. After leaves and nodules structure forming during IP process at first, larger leaves on CD-LDHs modified membranes will overlay the underneath nodules or overlap and merge to become belts [8]. Then a thinner but denser PA layer will be observed on

CD-LDHs modified membranes while a thicker but looser PA layer will form on CA-LDHs modified membranes.

However, the totally different result in CA-50 is notable. The ratio in Fig. 8b illustrates that a thinner PA layer was formed when CA-LDHs amount dramatically increase to 0.05%. This indicated that the diffusion of MPD shrank with the further addition of CA-LDHs. This can ascribe to the combination of CA-LDHs with each other. LDHs are easy to combine with each other, and when more CA-LDHs are added into aqueous phase, CA-LDHs unite to a dense layer and thus prevent MPD from diffusing to reaction zone.

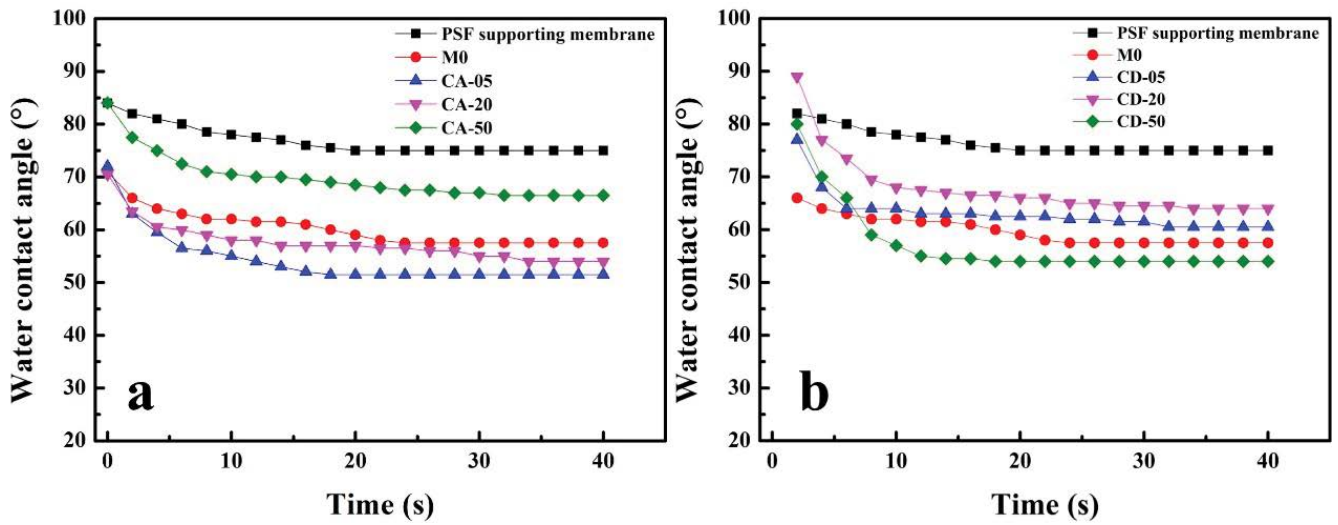


Fig. 7. Dynamic contact angle of LDHs modified membranes.

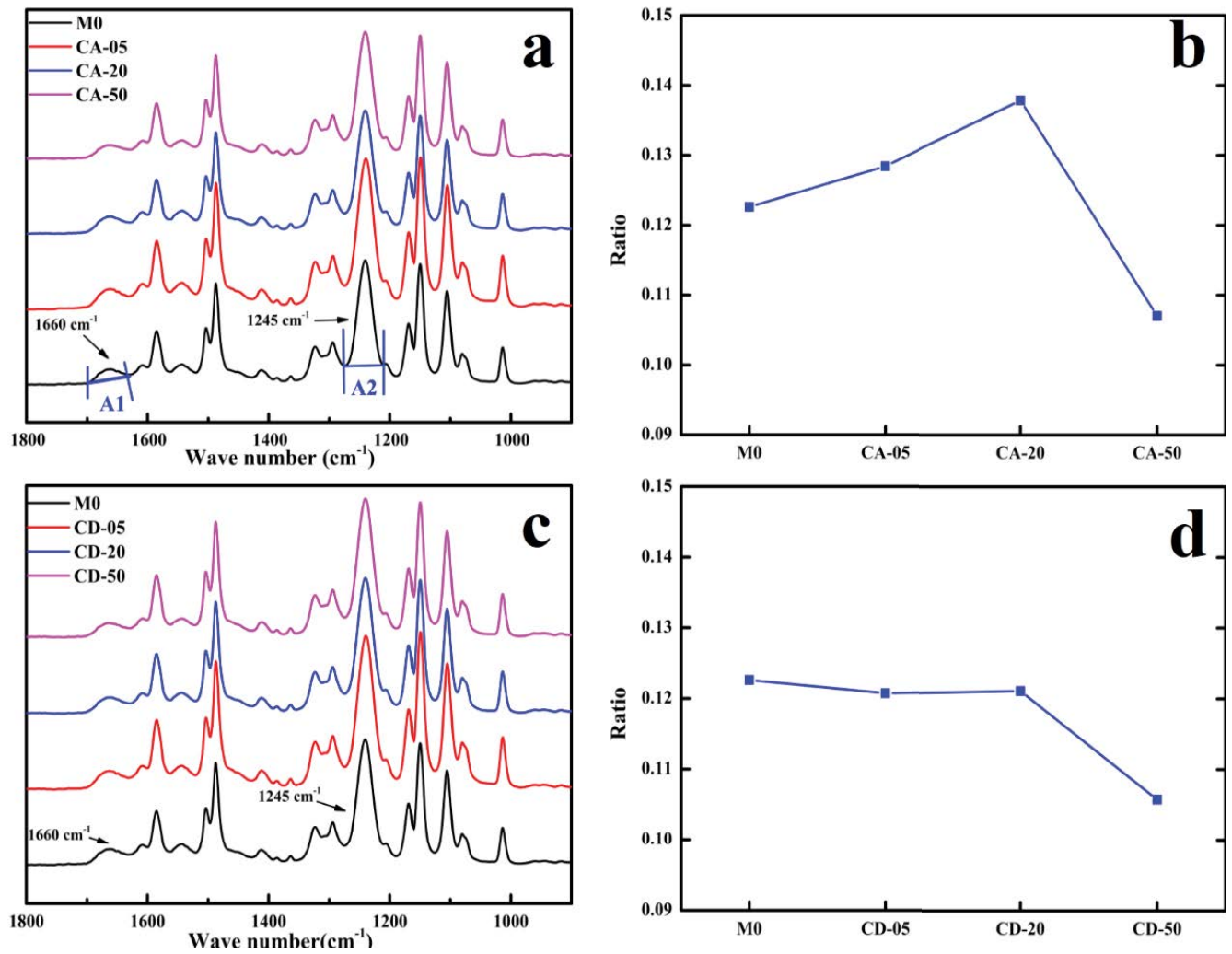


Fig. 8. ATR-FTIR spectra of RO membrane: (a and c) and area ratio of peaks at 1,660 and 1,245 cm^{-1} (b and d).

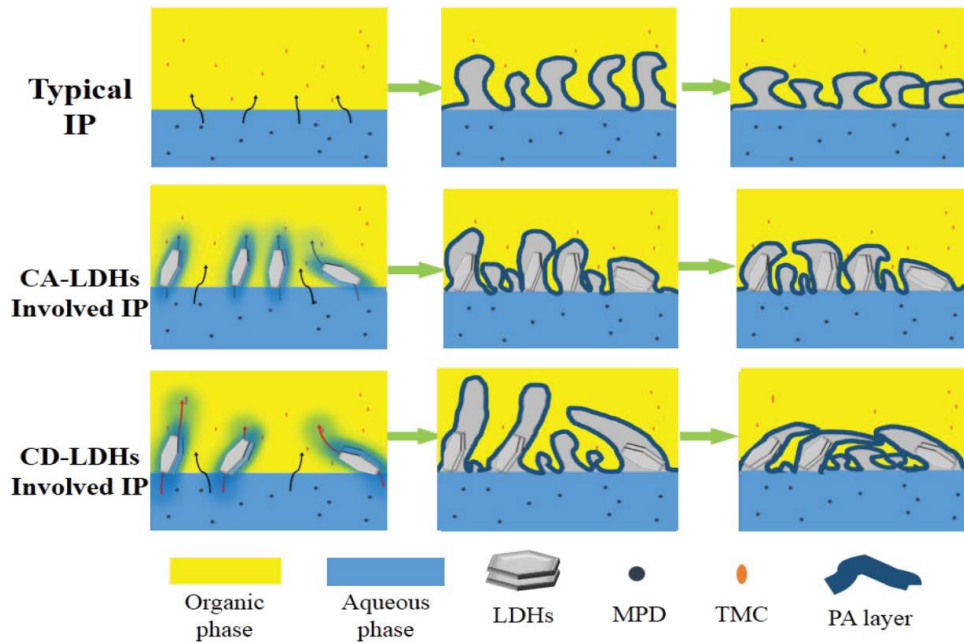


Fig. 9. IP process under different conditions.

3.3. Flux and rejection

The flux and rejection performance of RO membranes were evaluated by a cross-flow filtration system. As seen in Fig. 10, with the increase of CA-LDHs and CD-LDHs, both CA-LDHs and CD-LDHs modified membranes had an enhancement in flux at 0.005% added content. But both of the rejection of NaCl had a little decline, from 98.2% to 97.8% and 96.2%, respectively. When further increasing the amount of CA-LDHs and CD-LDHs, the performance of the membranes varied dramatically. The flux of CA-20 continued to increase to 33.2 L m⁻² h⁻¹, which was about 36% improvement compared with that of M0, while the CD-20 declined both in flux and rejection. The diverse performances of CA-20 and CD-20 can be attributed to the

diverse structures of the two membranes. CA-20 had a sparse leaf-like structure PA layer in which exist many cavities (Figs. 5 and 6), leading to a larger active area for permeation. However, CD-20 had a compact and dense circle slice structure, conducting a lower water permeability. And because of the existence of thinner PA layers where covered by no dense leaf-like PA, CD-20 also had more defects on it, leading to the decline in salt rejection. The water contact angle results also proved that CA-20 was more hydrophilic than CD-20, which principally ascribed to its sparse structure. Compared with CA-20 and CD-20, both CA-50 and CD-50 had an apparent fall in flux and rejection. Usually, a decline in rejection is inevitable to occur when a TFC membrane is modified with large amount of nanoparticles for

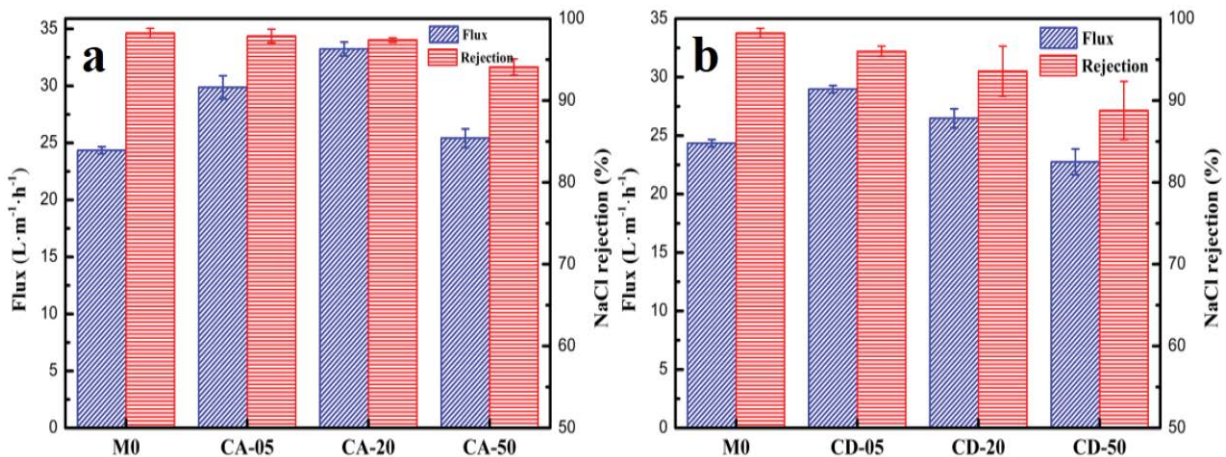


Fig. 10. Flux and NaCl rejection performance of (a) CA-LDHs modified membranes and (b) CD-LDHs modified membranes at 1.6 MPa. NaCl solution concentration: 2,000 mg/L.

the defects cause by the aggregation of nanoparticles. The decline in rejection of CA-50 and CD-50 can attribute to the same reason. Otherwise, the aggregation of LDHs also can block the membrane hole on PSF membrane, bringing out an enormous diminution of flux since the ATR-FTIR peak area ratio shows that a thinner layer is produced in CA-50 and CD-50. Unlike CA-05 and CA-20, both CD-05 and CD-20 have an evident decline in rejection. This recession of rejection can be attributed to the hydrolysis of TMC. Because of the existence of intercalated carbon dots, much more water is transported across the interface during the IP reaction and reacted with active TMC, resulting in a decline in degree of polymerization and crosslink, which is crucial to salt rejection.

4. Conclusions

In summary, two kinds of methodix LDHs with CA and CDs intercalated were prepared and incorporated into the polyamide separating layers of RO membranes via the IP process. The influences of LDH addition amount and the effects of intercalated anions were investigated. The SEM and TEM results revealed the LDHs added in aqueous phase changed the morphology of the membrane enormously. The membrane prepared by 0.02% (w/v) CA-LDHs in aqueous phase had the best separation performance of $33.2 \text{ L m}^{-2} \text{ h}^{-1}$ without sacrificing rejection, which was about 36% improvement in flux compared with the unmodified membrane. The improved flux ascribed to a sparser leaf-like structure on top surface with more effective permeating areas and an enhanced hydrophilicity. LDHs provided a substance transportation channel which facilitated water and MPD molecule to disperse across interface during the IP reaction, resulting in a variation in morphology. Unlike CA-LDHs modified membrane, CD-LDHs modified membrane had an obvious decline in rejection, caused by defects of thin PA layers and the hydrolysis of TMC with water which was further transported across the interface by hydrophilic intercalated CDs.

Acknowledgment

The authors gratefully acknowledge financial support from the National Natural Science Foundation of China (21978081).

References

- [1] H.F. Ridgway, J. Orbell, S. Gray, Molecular simulations of polyamide membrane materials used in desalination and water reuse applications: recent developments and future prospects, *J. Membr. Sci.*, 524 (2017) 436–448.
- [2] K.P. Lee, T.C. Arnot, D. Mattia, A review of reverse osmosis membrane materials for desalination-development to date and future potential, *J. Membr. Sci.*, 370 (2011) 1–22.
- [3] G.D. Kang, Y.M. Cao, Development of antifouling reverse osmosis membranes for water treatment: a review, *Water Res.*, 46 (2012) 584–600.
- [4] X.H. Ma, Z.K. Yao, Z. Yang, H. Guo, Z.L. Xu, C.Y. Tang, M. Elimelech, Nanofoaming of polyamide desalination membranes to tune permeability and selectivity, *Environ. Sci. Technol. Lett.*, 5 (2018) 123–130.
- [5] X.H. Ma, Z. Yang, Z.K. Yao, H. Guo, Z.L. Xu, C.Y. Tang, Interfacial polymerization with electrospayed microdroplets: toward controllable and ultrathin polyamide membranes, *Environ. Sci. Technol. Lett.*, 5 (2018) 117–122.
- [6] M.J.T. Raaijmakers, N.E. Benes, Current trends in interfacial polymerization chemistry, *Prog. Polym. Sci.*, 63 (2016) 86–142.
- [7] X.H. Ma, H. Guo, Z. Yang, Z.K. Yao, W.H. Qing, Y.L. Chen, Z.L. Xu, C.Y. Tang, Carbon nanotubes enhance permeability of ultrathin polyamide rejection layers, *J. Membr. Sci.*, 570–571 (2019) 139–145.
- [8] X. Ma, Z. Yang, Z. Yao, H. Guo, Z. Xu, C.Y. Tang, Tuning roughness features of thin film composite polyamide membranes for simultaneously enhanced permeability, selectivity and anti-fouling performance, *J. Colloid Interface Sci.*, 540 (2019) 382–388.
- [9] J.R. Werber, A. Deshmukh, M. Elimelech, The critical need for increased selectivity, not increased water permeability, for desalination membranes, *Environ. Sci. Technol. Lett.*, 3 (2016) 112–120.
- [10] G.R. Williams, D. O'Hare, Towards understanding, control and application of layered double hydroxide chemistry, *J. Mater. Chem.*, 16 (2006) 3065–3074.
- [11] Q. Wang, D. Ohare, Recent advances in the synthesis and application of layered double hydroxide (LDH) nanosheets, *Chem. Rev.*, 112 (2012) 4124–4155.
- [12] Y. Liu, N. Wang, J. Caro, *In situ* formation of LDH membranes of different microstructures with molecular sieve gas selectivity, *J. Mater. Chem. A*, 2 (2014) 5716–5723.
- [13] J. Wang, Y. Zhang, J. Zhu, J. Hou, J. Liu, B. Van der Bruggen, Zwitterionic functionalized layered double hydroxides nanosheets for a novel charged mosaic membrane with high salt permeability, *J. Membr. Sci.*, 510 (2016) 27–37.
- [14] Z. Shami, S.M. Amininasab, P. Shakeri, Structure-property relationships of nanosheeted 3D hierarchical roughness MgAl-layered double hydroxide branched to an electrospun porous nanomembrane: a superior oil-removing nanofabric, *ACS Appl. Mater. Interfaces*, 8 (2016) 28964–28973.
- [15] P. Lu, S. Liang, T. Zhou, X. Mei, Y. Zhang, C. Zhang, A. Umar, Q. Wang, Layered double hydroxide/graphene oxide hybrid incorporated polysulfone substrate for thin-film nanocomposite forward osmosis membranes, *RSC Adv.*, 6 (2016) 56599–56609.
- [16] G. Li, Z. Song, W. Liu, D. Yu, H. Wang, Alkyl ketene dimer emulsions stabilized by layered double hydroxide particles modified with glutamic acid, *Ind. Eng. Chem. Res.*, 56 (2017) 11435–11442.
- [17] F. Yang, S. Liu, J. Xu, Q. Lan, F. Wei, D. Sun, Pickering emulsions stabilized solely by layered double hydroxides particles: the effect of salt on emulsion formation and stability, *J. Colloid Interface Sci.*, 302 (2006) 159–169.
- [18] S. Abend, G. Lagaly, Bentonite and double hydroxides as emulsifying agents, *Clay Miner.*, 36 (2001) 557–570.
- [19] X. Tian, J. Wang, H. Zhang, Z. Cao, M. Zhao, Y. Guan, Y. Zhang, Establishment of transport channels with carriers for water in reverse osmosis membrane by incorporating hydrotalcite into the polyamide layer, *RSC Adv.*, 8 (2018) 12439–12448.
- [20] J.A. Gursky, S.D. Blough, C. Luna, C. Gomez, A.N. Luevano, E.A. Gardner, Particle-particle interactions between layered double hydroxide nanoparticles, *J. Am. Chem. Soc.*, 128 (2006) 8376–8377.
- [21] P.M. Pardeshi, A.K. Mungray, A.A. Mungray, Polyvinyl chloride and layered double hydroxide composite as a novel substrate material for the forward osmosis membrane, *Desalination*, 421 (2017) 149–159.
- [22] Y. Dong, J. Shao, C. Chen, H. Li, R. Wang, Y. Chi, X. Lin, G. Chen, Blue luminescent graphene quantum dots and graphene oxide prepared by tuning the carbonization degree of citric acid, *Carbon*, 50 (2012) 4738–4743.
- [23] W. Jia, B. Tang, P. Wu, Carbon dots with multi-functional groups and the application in proton exchange membranes, *Electrochim. Acta*, 260 (2018) 92–100.
- [24] D. Qu, M. Zheng, L. Zhang, H. Zhao, Z. Xie, X. Jing, R.E. Haddad, H. Fan, Z. Sun, Formation mechanism and optimization of highly luminescent N-doped graphene quantum dots, *Sci. Rep.*, 4 (2014) 5294.

- [25] S. Huang, X. Cen, H. Zhu, Z. Yang, Y. Yang, W.W. Tjiu, T. Liu, Facile preparation of poly(vinyl alcohol) nanocomposites with pristine layered double hydroxides, *Mater. Chem. Phys.*, 130 (2011) 890–896.
- [26] W. Liu, S. Xu, R. Liang, M. Wei, D.G. Evans, X. Duan, *In situ* synthesis of nitrogen-doped carbon dots in the interlayer region of a layered double hydroxide with tunable quantum yield, *J. Mater. Chem. C*, 5 (2017) 3536–3541.
- [27] J. Liao, Z. Wang, C. Gao, M. Wang, K. Yan, X. Xie, S. Zhao, J. Wang, S. Wang, A high performance PVAm-HT membrane containing high-speed facilitated transport channels for CO₂ separation, *J. Mater. Chem. A*, 3 (2015) 16746–16761.
- [28] M.M. Klosowski, C.M. McGilvery, Y. Li, P. Abellan, Q. Ramasse, J.T. Cabral, A.G. Livingston, A.E. Porter, Micro- to nano-scale characterisation of polyamide structures of the SW30HR RO membrane using advanced electron microscopy and stain tracers, *J. Membr. Sci.*, 520 (2016) 465–476.
- [29] T. Kamada, T. Ohara, T. Shintani, T. Tsuru, Optimizing the preparation of multi-layered polyamide membrane via the addition of a co-solvent, *J. Membr. Sci.*, 453 (2014) 489–497.
- [30] J. Xu, H. Yan, Y. Zhang, G. Pan, Y. Liu, The morphology of fully-aromatic polyamide separation layer and its relationship with separation performance of TFC membranes, *J. Membr. Sci.*, 541 (2017) 174–188.
- [31] V. Freger, Kinetics of film formation by interfacial polycondensation, *Langmuir*, 21 (2005) 1884–1894.
- [32] T. Kamada, T. Ohara, T. Shintani, T. Tsuru, Controlled surface morphology of polyamide membranes via the addition of co-solvent for improved permeate flux, *J. Membr. Sci.*, 467 (2014) 303–312.
- [33] B. Khorshidi, T. Thundat, B.A. Fleck, M. Sadrzadeh, A novel approach toward fabrication of high performance thin film composite polyamide membranes, *Sci. Rep.*, 6 (2016) 22069.
- [34] B. Khorshidi, T. Thundat, D. Pernitsky, M. Sadrzadeh, A parametric study on the synergistic impacts of chemical additives on permeation properties of thin film composite polyamide membrane, *J. Membr. Sci.*, 535 (2017) 248–257.

Supplementary information:

S1. Synthesis of standard LDHs

First, 0.02 mol Mg(NO₃)₂·6H₂O and 0.01 mol Al(NO₃)₃·9H₂O were dissolved in deionized water to form a 50 mL solution, which is named as solution A. 0.07 mol NaOH and 0.01 mol citric acid were dissolved in deionized water to form a 20 mL solution, and named it as solution B. Under rapid stirring, solution B was slowly added to solution A for co-precipitation, and the pH was controlled at 10. Then, the resulting suspension was transferred to a 100 mL teflon-lined autoclave and aged at 110°C for 24 h. After the suspension was cooled, the precipitate was centrifuged at 6,000 rpm, washed alternately with deionized water and ethanol, and dried at 60°C. The resulting product was standard citric acid (CA) intercalated Layered double hydroxides (LDHs), which was denoted as CA-W.

Disperse 0.4 g of CA-W in 40 mL of deionized water and add 0.2 mL of ethylenediamine. After ultrasonic dispersion for 30 min, the suspension was transferred to a 100 mL teflon-lined autoclave and heated at 150°C for 6 h. The product was separated at 7,500 rpm and washed alternately with deionized water and ethanol, and dried at 60°C. The resulting product was standard CD-LDHs, which was denoted as CD-W.

S2. Characterization

Denote methoxide CA-LDHs without water dispersion as CA-F, methoxide CD-LDHs without water dispersion as CD-F.

Fourier transform infrared (FT-IR) spectrum of CA-W and CD-W are shown in Fig. S1. Compared with Fig. 1, we can find that differences in infrared spectra of LDHs prepared by different methods are mainly concentrated at the wave number below 1,000 cm⁻¹, such as the wave number of 662 cm⁻¹, which can be ascribed to different crystal structures. Different crystal structures mean different covalent bond strength in the compound, which will lead to changes in absorption peak intensity, position shift and peak shape change.

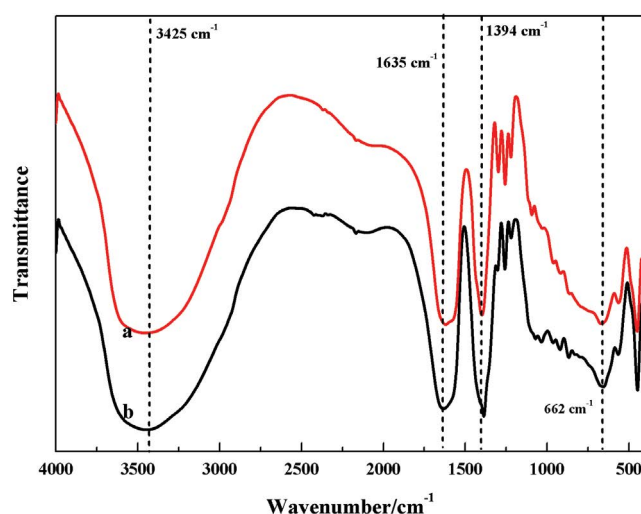


Fig. S1. FT-IR spectrum of (a) CA-W and (b) CD-W.

XRD spectrum of CA-F and CD-F are shown in Fig. S2. We can find that both CA-F and CD-F have no sharp peak on XRD, which means they are amorphous.

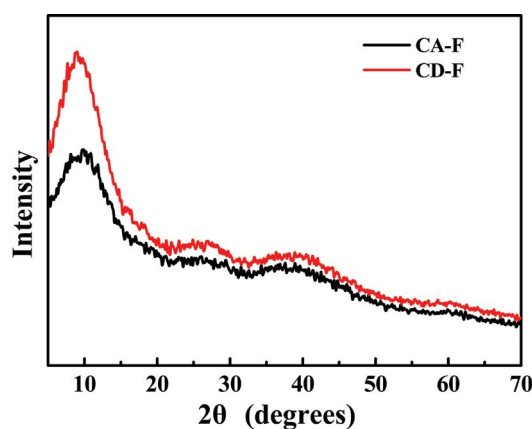


Fig. S2. XRD spectrum of CA-F and CD-F.

The SEM images of CA-W, CD-W, CA-F, and CD-F are shown in Fig. S3. CA-W and CD-W have the characteristic sheet structure of magnesium aluminum LDHs and a severe aggregation are observed on both CA-W and CD-W. Unlike

CA-LDHs and CD-LDHs in Fig. 3, CA-F and CD-F show an irregular granular structure, further indicating that before dispersing in water, methoxide LDHs are amorphous.

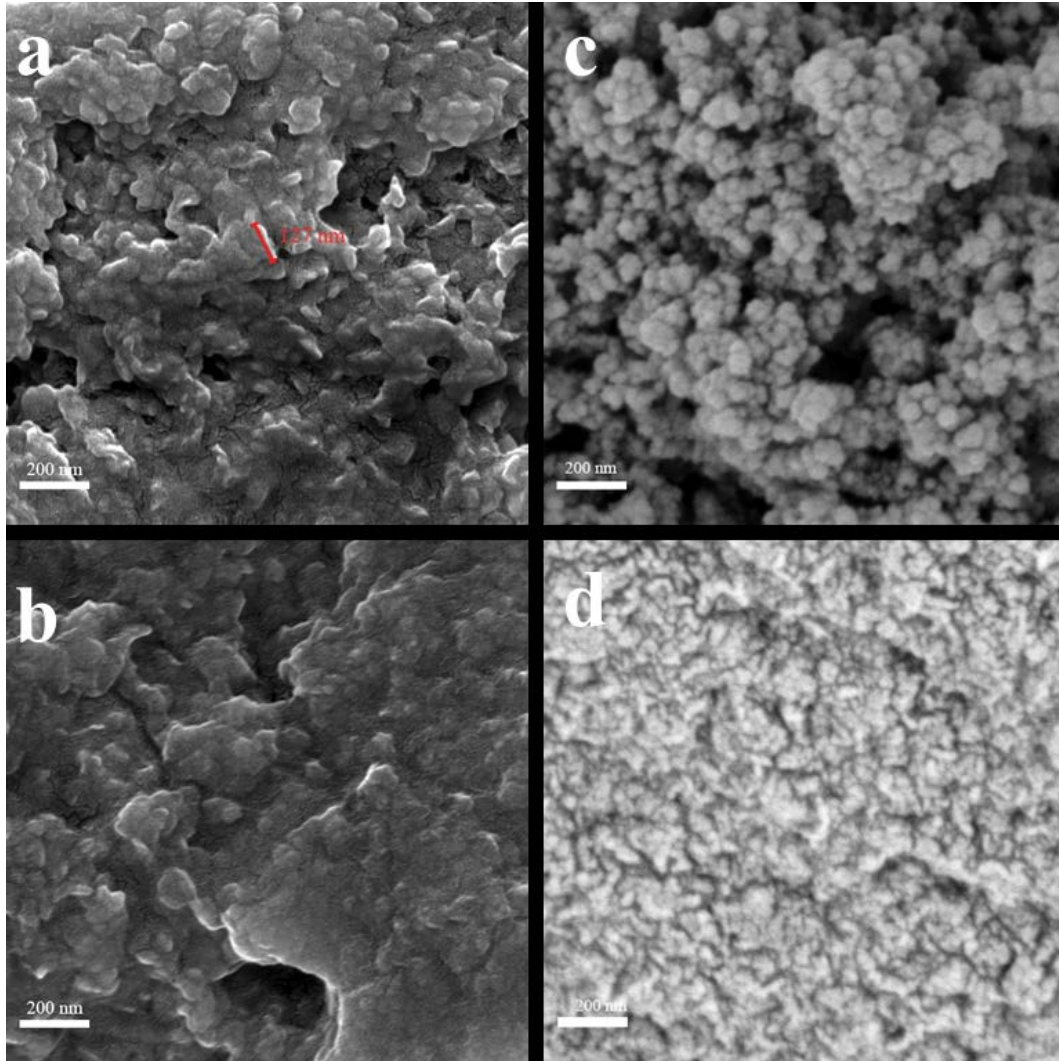


Fig. S3. SEM images of (a) CA-W, (b) CD-W, (c) CA-F, and (d) CD-F.